PERGAMON

International Journal of Heat and Mass Transfer 42 (1999) 4523–4534

International Journal of HEAT and MASS TRANSFER

www.elsevier.com/locate/ijhmt

Laminar natural convection heat and mass transfer in vertical rectangular ducts

Kuan-Tzong Lee

Department of Mechanical Engineering, Oriental Institute of Technology, Pan-Chiao, Taipei 22064, Taiwan, ROC

Received 29 October 1998; received in revised form 9 March 1999

Abstract

The present work investigates numerically the laminar natural convection heat and mass transfer in open vertical rectangular ducts with uniform wall temperature/uniform wall concentration (UWT/UWC) or uniform heat flux/uniform mass flux (UHF/UMF) boundary conditions. The vorticity–velocity formulation is applied to solve for the coupled momentum, energy and concentration equations. Results of dimensionless induced volume rate Q, average Nusselt number Nu and Sherwood number Sh are presented in terms of channel length L, buoyancy ratio N, Grashof number Gr, Schmidt number Sc and aspect ratio γ. Analytical solutions for Q, Nu and Sh for the UWT/UWC case are derived under fully developed condition. In addition, the correlation equations of Q, Nu and Sh for both boundary conditions are also presented.

1. Introduction

Transport processes in which the combined buoyancy forces of heat and mass transfer, resulting from the simultaneous presence of differences in temperature and variations in concentration, have significant influences on momentum, heat and mass in flowing gas mixtures are often encountered in many engineering system and the natural environment. The engineering applications include: the chemical reaction in reactor chamber, chemical vapor deposition of solid layers, cooling of electronic equipment, crystal growth. Similar processes occurring in nature also include various photosynthetic mechanisms, discharge into bodies of water, calm-day evaporation and vaporization of mist and fog and evaporation from and circulation in terrestrial bodies of water. The study of natural convection heat and mass concerned with external flows has been examined by numerous researchers. Bottemanne [1] obtained the solution of the natural convection heat and mass transfer along a vertical plate for the specified condition of $Pr = 0.71$ and $Sc = 0.63$. Detailed literature survey about natural convection heat and mass transfer along a vertical plate or a horizontal plate was presented by Gebhart and Pera [2,3]. They obtained a similarity solution for vertical [2] and horizontal [3] plates for the case of constant wall temperature and constant wall concentration. Gallahan and Marner [4] studied the effect of mass transfer on transient free convection flow past a semi-finite vertical isothermal plate for $Pr = 1$ and $Sc = 0.2$, 0.7 and 7. Soundalgeker and his colleagues [5,6] investigated the transient free convection with mass transfer along an infinite or a semi-infinite vertical plate in air flows with real gaseous species such as H, He, H_2O, NH_3 and CO_2 ($Sc = 0.16$, 0.3, 0.6, 0.68 and 1.0). Natural convection heat and mass transfer along an inclined plate or a vertical cylinder was reported by Chen and Yuh [7,8] for various fluid flow. These analyses were based on species diffusion processes with very low concentration levels such that the

E-mail address: fd006@ica.oit.edu.tw (K.T. Lee)

0017-9310/99/$ - see front matter
PII: S0017-9310(99)00101-5

Nomenclature

a, b	width and depth of the rectangular duct, respectively [m]
A	cross-sectional area of the vertical rectangular duct [m^2]
c_p	specific heat of fluid [J kg^{-1} K^{-1}]
C, c	dimensionless and dimensional species mass fraction, $C=(c-c_0)/(c_w-c_0)$ for UWT/UWC or $(c-c_0)/(m_w D_e/D)$ for UHF/UMF
C_1, C_2	constants in correlation equations
D	mass diffusivity [m^2 s^{-1}]
D_e	equivalent hydraulic diameter, $4A/S$ [m]
g	gravitational acceleration [m s^{-2}]
Gr	Grashof number, $g\beta\Delta T D_e^4/l\nu^2$
h_m	average convective heat transfer coefficient
I, J	number of finite difference divisions in the X- and Y-directions, respectively
k	thermal conductivity [W m^{-1} K^{-1}]
L, l	dimensionless and dimensional length of the vertical duct, $L = 1/Gr$
Le	Lewis number, Sc/Pr
n	dimensionless direction coordinate normal to the duct walls
N	buoyancy ratio, $\beta^*(c_w-c_0)/\beta(T_w-T_0)$ for UWT/UWC or $(\beta^* m_w/D)/(\beta q_w/k)$ for UHF/UMF
Nu	average Nusselt number
Nu_z	local Nusselt number
$\bar{P}, \bar{p}$	dimensionless and dimensional cross-sectional mean pressure, $\bar{P}=\bar{p}/(\rho w_0^2)$
Pr	Prandtl number, ν/α
q_w	wall heat flux [W m^{-2}]
Q	dimensionless volume flow rate
$\bar{Q}, \dot{q}$	dimensionless and dimensional heat transfer rate
S	circumference of cross-section [m]
Sc	Schmidt number, ν/D
Sh	average Sherwood number
Sh_z	local Sherwood number
T	temperature [K]
u, v, w	velocity components in x-, y- and z-directions, respectively [m s^{-1}]
U, V, W	dimensionless velocity components in x-, y- and z-directions, respectively, $U=uD_e/\nu$, $V=vD_e/\nu$, $W=wD_e^2/l\nu\,Gr$
w_0	mean velocity at the entrance [m s^{-1}]
x, y, z	coordinate system [m]
X, Y, Z	dimensionless coordinate system, $X=x/D_e$, $Y=y/D_e$, $Z=z/(l\,Gr)$
Z^*	scale parameter of fully-developed flow, $1+N/Le$.

Greek symbols

α	thermal conductivity [m^2 s^{-1}]
β	coefficient of thermal expansion
β^*	coefficient of concentration expansion
γ	aspect ratio, a/b
ΔT	characteristics temperature difference, (T_w-T_0) for UWT/UWC or $q_w D_e/k$ for UHF/UMF
θ	dimensionless temperature, $(T-T_0)/\Delta T$
ν	kinematic viscosity [m^2 s^{-1}]
ξ	dimensionless vorticity in the z-direction
ρ	fluid density [kg m^{-3}].

Subscripts

w	value at wall
0	condition at inlet.

Soret–Dufour (thermo diffusion and diffusion-thermo) effects, as well as the interfacial velocity at the wall due to species diffusion, were neglected. Srinivasan and Angirasa [9] presented the complex interaction of natural convection heat and mass transfer between Schmidt number, buoyancy ratio and stratification parameters in unsteady double-diffusive free convection flow along a vertical surface. Lin and Wu [10,11] obtained nonsimilarity results for most practical solutions ($Pr = 0.7$, $0.21 \le Sc \le 2.1$) and aqueous solutions ($Pr = 7$, $0.21 \le Sc \le 2.1$). They also proposed correlation equations for estimating the rates of heat and mass transfer along a vertical plate.

The heat and mass transfer in a channel flow has received considerable attention. Gill et al. [12] considered combined free and forced convection for fully developed flow between inclined parallel plates with asymmetric mass transfer. A similarity solution was obtained by Mollendof and Gebhart [13] to examine the double diffusive free convection in the asymmetric case. The similarity solutions have a serious limitation since they can be obtained for a specific boundary condition only. Lee et al. [14] presented the results of natural convection heat and mass transfer between vertical parallel plates in which mass transfer from one wall resulted in a downward flow. Nelson and Wood

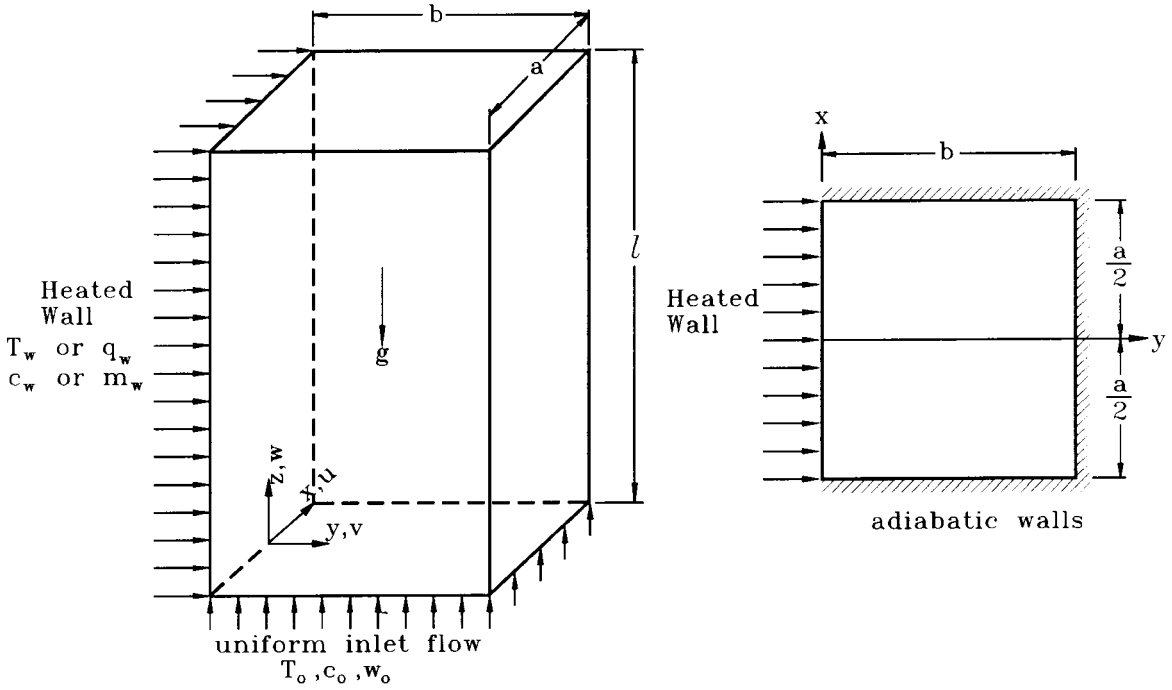

Fig. 1. Schematic diagram of the physical model.

[15,16] investigated numerically the combined heat and mass transfer for natural convection between vertical parallel plates. Their results cover a wide range of Rayleigh numbers from fully developed flow up to backflow of the exit for both aiding and opposing buoyancy cases due to mass transfer. Analytical solution for fully developed flow for the same problem was presented by Nelson and Wood [17].

As seen, few studies on the natural convection heat and mass transfer in vertical rectangular ducts exist in the open literature. This motivated the present study. Combined numerical and theoretical analyses were performed to investigate the natural convection heat and mass transfer in vertical rectangular ducts. A schematic of the flow configuration and coordinate system is illustrated in Fig. 1. The rectangular duct is opened to ambient at the top and bottom. The duct is of finite length l and having a width a (in the x-direction) and depth b (in the y-direction). In this work, a uniform wall temperature/uniform wall concentration (UWT/UWC) or a uniform heat flux/uniform mass flux (UHF/UMF) condition is imposed at one wall ($y = 0$), while the other walls are assumed to be adiabatic. At the duct inlet ($z = 0$), the buoyancy-induced flow is assumed to have uniform axial velocity w_0, uniform temperature T_0 and uniform concentration c_0.

2. Analysis

To simplify the analysis, the following assumptions are made: (1) the flow is assumed to be laminar, steady, boundary-layer type and of constant properties except the density variation of the buoyancy term in the z-momentum equation; (2) the Boussinesq approximation is used to characterize the buoyancy effects; (3) the viscous dissipation effect is negligible; and (4) the surface normal velocity is ignored due to the small temperature and concentration difference [7,8].

Based on the above assumptions, the dimensionless governing equations of the vorticity–velocity formulation can be expressed as [18]

$$\frac{\partial^2 U}{\partial X^2}+\frac{\partial^2 U}{\partial Y^2}=\frac{\partial \xi}{\partial Y}-\frac{\partial^2 W}{\partial X\,\partial Z} \tag{1}$$

$$\frac{\partial^2 V}{\partial X^2}+\frac{\partial^2 V}{\partial Y^2}=-\frac{\partial \xi}{\partial X}-\frac{\partial^2 W}{\partial Y\,\partial Z} \tag{2}$$

$$U\frac{\partial \xi}{\partial X}+V\frac{\partial \xi}{\partial Y}+W\frac{\partial \xi}{\partial Z}+\xi\left(\frac{\partial U}{\partial X}+\frac{\partial V}{\partial Y}\right)+\left(\frac{\partial W}{\partial Y}\right)\times\left(\frac{\partial U}{\partial Z}\right)-\left(\frac{\partial W}{\partial X}\right)\left(\frac{\partial V}{\partial Z}\right)=\left(\frac{\partial^2 \xi}{\partial X^2}+\frac{\partial^2 \xi}{\partial Y^2}\right) \tag{3}$$

$$U\frac{\partial W}{\partial X}+V\frac{\partial W}{\partial Y}+W\frac{\partial W}{\partial Z}=-\frac{\mathrm{d}\bar{P}}{\mathrm{d}Z}+\frac{\partial^2 W}{\partial X^2}+\frac{\partial^2 W}{\partial Y^2}+\theta+NC \tag{4}$$

$$U\frac{\partial \theta}{\partial X}+V\frac{\partial \theta}{\partial Y}+W\frac{\partial \theta}{\partial Z}=\frac{1}{Pr}\left(\frac{\partial^2 \theta}{\partial X^2}+\frac{\partial^2 \theta}{\partial Y^2}\right) \tag{5}$$

$$U\frac{\partial C}{\partial X}+V\frac{\partial C}{\partial Y}+W\frac{\partial C}{\partial Z}=\frac{1}{Sc}\left(\frac{\partial^2 C}{\partial X^2}+\frac{\partial^2 C}{\partial Y^2}\right) \tag{6}$$

where $\xi=\partial U/\partial Y-\partial V/\partial X$ is the dimensionless axial vorticity.

The governing equations are subjected to the following boundary conditions:

$$U=V=0,\quad W=1,\quad \theta=C=0 \quad \text{(at the inlet } Z=0)$$

$$U=V=W=0,\quad \partial\theta/\partial n=\partial C/\partial n=0$$

(at the wall $X=-(1+\gamma)/4$)

$$U=V=W=0,\quad \partial\theta/\partial n=\partial C/\partial n=0$$

(at the wall $X=(1+\gamma)/4$)

$$U=V=W=0,\quad \theta=C=1 \quad \text{(at the wall } Y=0)$$

for UWT/UWC

$$U=V=W=0,\quad \partial\theta/\partial n=\partial C/\partial n=-1$$

(at the wall $Y=0$) for UHF/UMF

$$U=V=W=0,\quad \partial\theta/\partial n=\partial C/\partial n=0$$

(at the wall $Y=(1+\gamma)/2\gamma$) (7)

In this work, the variables of interest are the induced volume flow rate, the average Nusselt and Sherwood numbers. The dimensionless induced volume flow rate is defined as

$$Q=\int_0^{(1+\gamma)/2\gamma}\int_{-(1+\gamma)/4\gamma}^{(1+\gamma)/4\gamma} W\,\mathrm{d}X\,\mathrm{d}Y \tag{8}$$

The average Nusselt number is the mean value of the local Nusselt number on the heated wall, i.e.

$$Nu=\frac{1}{L}\int_0^L Nu_z\,\mathrm{d}Z \tag{9a}$$

where

$$Nu_z=\frac{2}{1+\gamma}\int_{-(1+\gamma)/4}^{(1+\gamma)/4}-\left.\frac{\partial\theta}{\partial Y}\right|_{Y=0}\mathrm{d}X \tag{9b}$$

(UWT/UWC)

$$Nu_z=\frac{2}{1+\gamma}\int_{-(1+\gamma)/4}^{(1+\gamma)/4}-\left.\frac{1}{\theta}\right|_{Y=0}\mathrm{d}X \quad \text{(UHF/UMF)} \tag{9c}$$

Similarly, the average Sherwood number is defined as

$$Sh=\frac{1}{L}\int_0^L Sh_z\,\mathrm{d}Z \tag{10a}$$

where

$$Sh_z=\frac{2}{1+\gamma}\int_{-(1+\gamma)/4}^{(1+\gamma)/4}-\left.\frac{\partial C}{\partial Y}\right|_{Y=0}\mathrm{d}X \tag{10b}$$

(UWT/UWC)

$$Sh_z=\frac{2}{1+\gamma}\int_{-(1+\gamma)/4}^{(1+\gamma)/4}-\left.\frac{1}{C}\right|_{Y=0}\mathrm{d}X \quad \text{(UHF/UMF)} \tag{10c}$$

3. Analytical solution

Before beginning the general numerical solution, the analytical solutions for low Grashof number limit, i.e. fully developed flow, in the case of UWT/UWC, are first obtained. These solutions, although only approximate, provide useful data against which the computed results can be checked. Under the assumption of fully-developed flow, differentiating Eq. (4) twice with respect to X and Y and combining Eqs. (5) and (6) leads to

$$\frac{\partial^4 W}{\partial X^4}+2\frac{\partial^4 W}{\partial X^2\partial Y^2}+\frac{\partial^4 W}{\partial Y^4}+Pr\,W\frac{\partial\theta}{\partial Z}+N\,Sc\,W\frac{\partial\partial C}{\partial Z}=0 \tag{11}$$

In the case of uniform wall temperature/uniform wall concentration (UWT/UWC), the terms of $\partial\theta/\partial Z$ and $\partial\theta/\partial Z$ are zero. Hence, Eq. (11) can be reduced to be

$$\frac{\partial^4 W}{\partial X^4} + 2\frac{\partial^4 W}{\partial X^2 \partial Y^2} + \frac{\partial^4 W}{\partial Y^4} = 0 \tag{12}$$

The solution of Eq. (12) has the form

$$W = W_1(Y) + W_2(X, Y) \tag{13}$$

where

$$W_1 = \frac{1+N}{2}\left(\frac{1+\gamma}{2\gamma}Y - Y^2\right) \tag{14}$$

In Eq. (14), the W_1 represents the velocity distribution on the symmetric axis $X = 0$, which is identical to the result of parallel plate flow [17]. Now, we can express the W_1 in a trigonometric series:

$$W_1 = \frac{(1+\gamma)^2(1+N)}{2\gamma^2\pi^3}\sum_{m=1}^{\infty}\frac{1}{m^3}\left[2\sin\left(\frac{m\pi}{2}\right) - m\pi\cos\left(\frac{m\pi}{2}\right)\right]\sin\left(\frac{m\pi}{2}\right)\sin\left(\frac{2\gamma m\pi Y}{1+\gamma}\right) \tag{15}$$

On the other hand, let $W_2(X, Y)$ be the following series form:

$$W_2 = \sum_{m=1}^{\infty} X_m \sin\left(\frac{2\gamma m\pi Y}{1+\gamma}\right) \tag{16}$$

where X_m is a function of X only. Introducing W_2 into Eq. (12) yields a fourth-order O.D.E.:

$$X_m^{\mathrm{IV}} - 2m^2\pi^2 X_m + m^4\pi^4 X_m = 0 \tag{17}$$

Since the velocity profile in the cross section of a duct is symmetric with respect to the Y axis, the general solution of X_m can be expressed as

$$X_m = A_m \cosh\left(\frac{2\gamma m\pi X}{1+\gamma}\right) + \frac{2\gamma m\pi X}{1+\gamma}B_m \sinh\left(\frac{2\gamma m\pi X}{1+\gamma}\right) \tag{18}$$

Combination of Eqs. (16) and (18) yields the solution of W_2. Finally, the solution for the velocity profile in the cross section of the rectangular duct can then be found by the summation of W_1 and W_2, i.e.

$$W = \sum_{m=1}^{\infty}\left\{\frac{(1+\gamma)^2(1+N)}{2\gamma^2 m^3\pi^3}\left[2\sin\left(\frac{m\pi}{2}\right) - m\pi\cos\left(\frac{m\pi}{2}\right)\right]\sin\left(\frac{m\pi}{2}\right) + A_m\cosh\left(\frac{2\gamma m\pi X}{1+\gamma}\right) + m\pi\frac{2\gamma m\pi X}{1+\gamma}B_m\sinh\left(\frac{2\gamma m\pi X}{1+\gamma}\right)\right\}\sinh\left(\frac{2\gamma m\pi Y}{1+\gamma}\right) \tag{19}$$

Substituting boundary conditions of $W = 0$ on the side walls $X = \pm\gamma/2$ into the above equation, we can find the velocity profile

$$W = \frac{(1+\gamma)^2(1+N)}{\gamma^3\pi^3}\sum_{m=1,\,3,\,5,\,\ldots}^{\infty}\frac{1}{m^3}\left[-\cosh\left(\frac{\gamma m\pi}{2}\right) + \cosh\left(\frac{2\gamma m\pi X}{1+\gamma}\right)\right]\mathrm{sech}\left(\frac{\gamma m\pi}{2}\right)\sin\left(\frac{2\gamma m\pi Y}{1+\gamma}\right) \tag{20}$$

According to the definition of Eq. (8), the dimensionless induced volume rate under fully-developed limit can be derived by inserting the known velocity profile, Eq. (20), into the integral of Eq. (8). This leads to

$$Q = \int_0^{(1+\gamma)/2\gamma}\int_{-(1+\gamma)/4}^{(1+\gamma)/4} W\,\mathrm{d}X\,\mathrm{d}Y = -\frac{(1+\gamma)^4(1+N)}{2\gamma^4\pi^5}\sum_{m=1,\,3,\,5\ldots}^{\infty}\frac{1}{m^5}\mathrm{sech}\left(\frac{\gamma m\pi}{2}\right) \times\left[2\sinh\left(\frac{\gamma m\pi}{2}\right) - \gamma m\pi\cosh\left(\frac{\gamma m\pi}{2}\right)\right] \tag{21}$$

It is worth noting in Eq. (21) that the dimensionless induced volume rate Q is independent of the parameters of Pr and Sc for fully-developed flow. The heat absorbed by the fluid rising in the rectangular duct is given by

$$\dot{q} = \rho c_{\mathrm{p}}\int_0^b\int_{-a/2}^{a/2} w(T - T_0)\,\mathrm{d}x\,\mathrm{d}y \tag{22}$$

The above equation can be rewritten in a dimensionless form as

$$\dot{Q} = \frac{\dot{q}}{\rho c_{\mathrm{p}}\nu l\,Gr(T_{\mathrm{w}} - T_0)} = \int_0^{(1+\gamma)/2\gamma}\int_{-(1+\gamma)/4}^{(1+\gamma)/4} W\theta\,\mathrm{d}X\,\mathrm{d}Y \tag{23}$$

An average surface conductance over the heated wall can be defined by

$$h_{\mathrm{m}} = \frac{\dot{q}}{al(T_{\mathrm{w}} - T_0)} \tag{24}$$

The average Nusselt number is defined by

$$Nu = \frac{h_{\mathrm{m}}D_{\mathrm{e}}}{k} \tag{25}$$

Therefore, from Eqs. (23)–(25), we can find the average Nusselt number under the fully-developed flow condition:

$$Nu = \frac{2}{1+\gamma} Pr\, Gr \int_0^{(1+\gamma)/2\gamma} \int_{-(1+\gamma)/4}^{(1+\gamma)/4} W\theta \, dX \, dY$$

$$= \frac{2}{1+\gamma} Pr\, Gr\, Q \tag{26}$$

Similarly, the average Sherwood number can be obtained as

$$Sh = \frac{2}{1+\gamma} Sc\, Gr \int_0^{(1+\gamma)/2\gamma} \int_{-(1+\gamma)/4}^{(1+\gamma)/4} WC \, dX \, dY$$

$$= \frac{2}{1+\gamma} Sc\, Gr\, Q \tag{27}$$

4. Solution method

The present problem is numerically solved by the vorticity–velocity method for three-dimensional parabolic flow [18,19] in which the equations for unknown U, V, W, ξ, θ, and C are coupled. For a given condition, the field solutions are calculated by a marching technique based on the Du Fort Frankel scheme [20]. Details of the solution procedure have been described elsewhere [21,22] and are not repeated herein.

To insure the independence of the numerical results, a numerical experiment was made on the grid line $I \times J$ and axial step size ΔZ. Grids were chosen to be uniform in the cross-sectional direction but nonuniform in the axial flow direction to account for the uneven variations of W, θ and C near the inlet and exit. In the flow direction, grids are of highest density near the entrance and exit of the channel. In the present study, 41×41 nodes in the cross-section plane were used, while the number of nodes in the z-direction ranges from 1175 to 5475 ($\Delta Z = 1 \times 10^{-3}$–$5 \times 10^{-2} L$), depending on the Grashof number (i.e. channel length). To check the grid independence, a numerical experiment for the typical case ($N = 1$, $Pr = 0.7$, $Sc = 0.6$, $Gr = 10$ and $\gamma = 1$) with the boundary condition of UWT/UWC was made to determine the grid spacing and axial step size required for acceptable numerical accuracy. It is found in the separate numerical runs that the deviations in Nu and Sh calculated using either $I \times J = 41 \times 41$ or 61×61 are always within 2%. Furthermore, the deviations in local Nu and Sh calculated using either $I \times J\ (\Delta Z) = 41 \times 41$ (1×10^{-3}–$5 \times 10^{-2} L$) or 41×41 (5×10^{-4}–$3 \times 10^{-2} L$) are less than 1%. Accordingly, the computation involving an $I \times J\ (\Delta Z) = 41 \times 41$ (1×10^{-3}–$5 \times 10^{-2} L$) grid is considered to be sufficiently accurate to describe the natural convection heat and mass transfer in vertical ducts. As a partial verification of the computational procedure, results were initially obtained for pure natural convection heat transfer in vertical rectangular ducts ($N = 0$). The results of average Nusselt number were compared with those by Ramakrishna et al. [18] for a square duct and Moutsoglou and Park [23] for a rectangular duct. The Nusselt number was found to agree with those of Refs. [18,23] within 1%. To further validate the adequacy of the numerical solutions, the predictions of extremely large aspect ratio $\gamma = 40$ are compared to those obtained by Nelson and Wood [15]. It was found that the present predictions are in good agreement with those of Ref. [15]. The above numerical tests indicate that the solution procedure adopted is suitable for the present study.

5. Results and discussion

Inspection of the preceding analysis reveals that the characteristics of the natural convection heat and mass transfer in vertical rectangular ducts depend on five dimensionless groups: namely, the buoyancy ratio N, the Schmidt number Sc, the Grashof number Gr, the aspect ratio γ and the Prandtl number Pr. In the present analysis, to concentrate on the understanding

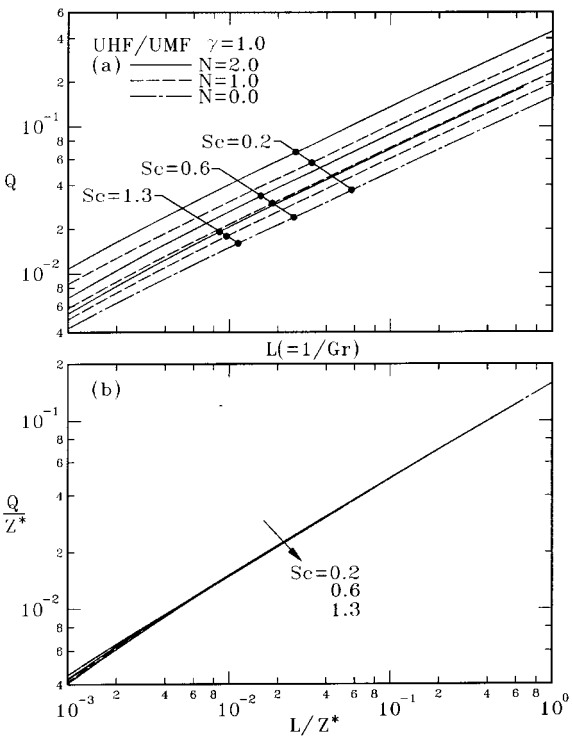

Fig. 2. Effects of buoyancy ratio N and Schmidt number Sc on the dimensionless induced volume rate for the case of UHF/UMF with $\gamma = 1$.

of heat and mass transfer characteristics, all the numerical runs were performed for $Pr = 0.7$. Schmidt number Sc is chosen to have the value of 0.2 (hydrogen), 0.6 (water vapor) and 1.3 (ethyl alcohol) for the buoyancy ratio N ranging from 0 to 2. The calculations of the governing equations yield the velocity, temperature and concentration profiles and the distribution of motion pressure along the flow direction. The results of practical interest are the induced volume flow rate, the average Nusselt and Sherwood numbers.

The effects of the buoyancy ratio N and the Schmidt number Sc on the dimensionless induced volume rate Q, the average Nusselt number Nu and the average Sherwood number Sh are shown, respectively, in Figs. 2, 4 and 6 for the uniform heat flux/uniform mass flux (UHF/UMF) case. Similar plots for the uniform wall temperature/uniform wall concentration (UWT/UWC) case are shown, respectively, in Figs. 3, 5 and 7. In these figures, $N = 0$ corresponds to the situation in which the natural convection arises from thermal buoyancy force only and there is no contribution from the species diffusion. The Q, Nu and Sh are therefore independent of the Schmidt number, as expected. When the buoyancy force from the species diffusion assists the thermal buoyancy force ($N > 0$), it is revealed that the Q, Nu and Sh increase with increasing N. It is also well known that a smaller Schmidt number corresponds to a larger binary diffusion coefficient, which in turn, exerts a larger influence on the flow field and hence the thermal field.

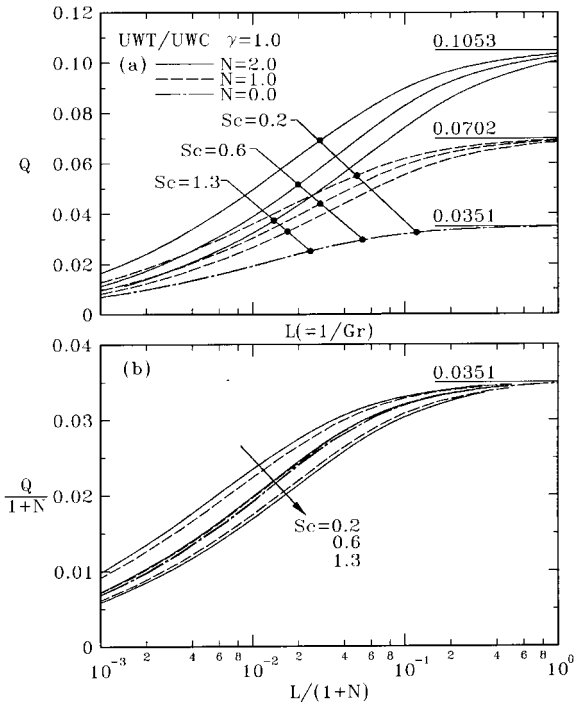

Fig. 3. Effects of buoyancy ratio N and Schmidt number Sc on the dimensionless induced volume rate for the case of UWT/UWC with $\gamma = 1$.

In Figs. 2(a) and 3(a), an increase in Sc causes a decrease in Q for a fixed value of N. This is due to the fact that as the Sc increases, the thickness of the concentration boundary layer decreases. This causes the flow driven by the concentration gradient to be confined closer to the wall. This leads to a lower axial velocity which in turn causes a lower volume flow rate. For the UWT/UWC case [see Fig. 3(a)], the Q increases with the channel length L and finally approaches an asymptotic value corresponding to the limit of fully-developed flow. Additionally, for a fixed Sc, the difference in Q between various N becomes significant as L is increased. It is also noted in Fig. 3(a) that the Q under fully-developed flow is independent of Sc for a fixed value of N. The volume flow rate of fully developed flow limit is 0.0351, 0.0702 and 0.1053 for $N = 0$, 1 and 2, respectively. Unlike the result of the UWT/UWC case, no fully developed flow limit is reached for the UHF/UMF case [see Fig. 2(a)]. This is because the driving force is sustained for the UHF/UMF case. The trend of the curves for various combinations of N and Sc is almost similar to each other. A comparison of Q between UHF/UMF and UWT/UWC cases shows that the UHF/UMF causes a higher Q than that of UWT/UWC for fully developed flow (i.e. a larger channel length) and the discrepancy is increased with increasing channel length. A careful inspection reveals that the trend is reversed for the case of a smaller channel length. Additionally, the discrepancy of Q between various values N (for a fixed Sc) and Sc (for a fixed N) is more significant in the UHF/UMF case. In Fig. 2(b), if the Q and L are scaled by the factor Z^* ($= 1 + N/Le$), then the results of Q/Z^* against L/Z^* nearly converge to a universal curve, except for the system with a smaller channel length. To facilitate the applications of the results, the correlation equation of Q for the UHF/UMF case is given here:

$$\frac{Q}{Z^*} = \frac{0.29122\eta^{0.545}}{(1 + 1.9746\eta^{0.018})^{1/1.8}} \quad \text{(UHF/UMF)} \tag{28}$$

where $\eta = L/Z^*$ and $Z^* = 1 + N/Le$. In Fig. 3(b), for the UWT/UWC case, if the Q and L are scaled by a factor $(1 + N)$, then the scaled values of $Q/(1 + N)$ at large $(L/(1 + N)$ become 0.0351 and are independent of N and Sc. This is in line with the analytical results in Eq. (21). The correlation equation of $Q/(1 + N)$ vs $L/(1 + N)$ can be given by

$$\frac{Q}{1 + N} = \frac{C_1\eta^{0.75}}{(1 + C_2\eta^{0.9375})^{1/1.8}} \quad \text{(UWT/UWC)} \tag{29}$$

Table 1
Constants of correlation equations for volume flow rate Q, the average Nusselt number Nu and the Sherwood number Sh for the UWT/UWC case

		$Sc = 0.2$		$Sc = 0.6$		$Sc = 1.3$	
		C_1	C_2	C_1	C_2	C_1	C_2
Q	$N = 0$	1.0161	66.531	1.0161	66.531	1.0161	66.531
	$N = 1$	1.4631	105.86	1.0679	70.715	0.81496	50.337
	$N = 2$	1.6307	120.66	1.1119	74.949	0.77142	47.211
Nu	$N = 0, 1, 2$	0.025779	0.0050237	0.023626	0.0050237	0.021860	0.0050237
Sh	$N = 0$	0.014727	0.0046032	0.017766	0.0046032	0.018456	0.0046032
	$N = 1$	0.020674	0.0046032	0.020846	0.0046032	0.020845	0.0046032
	$N = 2$	0.023584	0.0046032	0.022665	0.0046032	0.022361	0.0046032

where $\eta = L/(1+N)$ and the constants C_1 and C_2 are listed in Table 1.

It is clear in Figs. 4(a) and 5(a) that the smaller Nu is experienced for a system with a higher Sc. This is due to the fact that the increase in Sc causes a decrease in flow velocity and hence diffusion dominates over convection. In Fig. 5(a), for the UWT/UWC case, the Nu under fully-developed flow limit (i.e. a small Gr case) is independent of Sc for a fixed value of N. But the curves for various Sc branch off each other at higher Gr, and the value of Nu decreases with increasing Sc. Similar to the results of induced volume flow

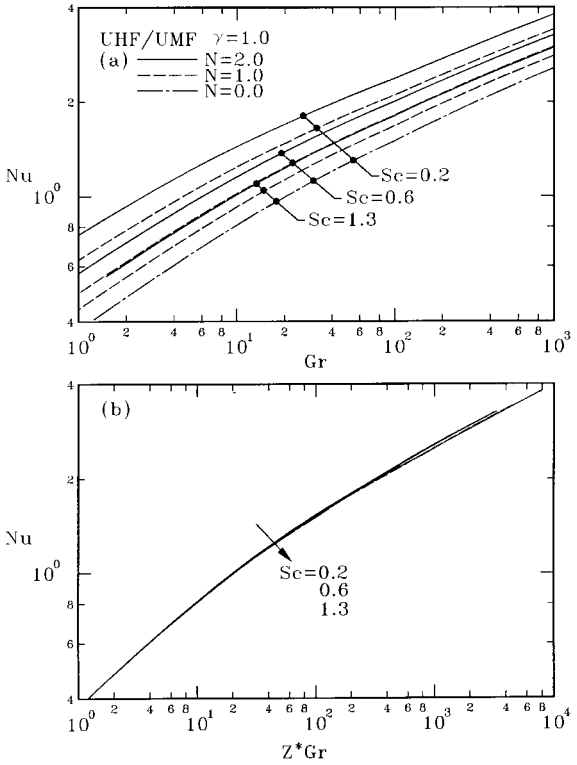

Fig. 4. Effects of buoyancy ratio N and Schmidt number Sc on the average Nusselt number for the case of UHF/UMF with $\gamma = 1$.

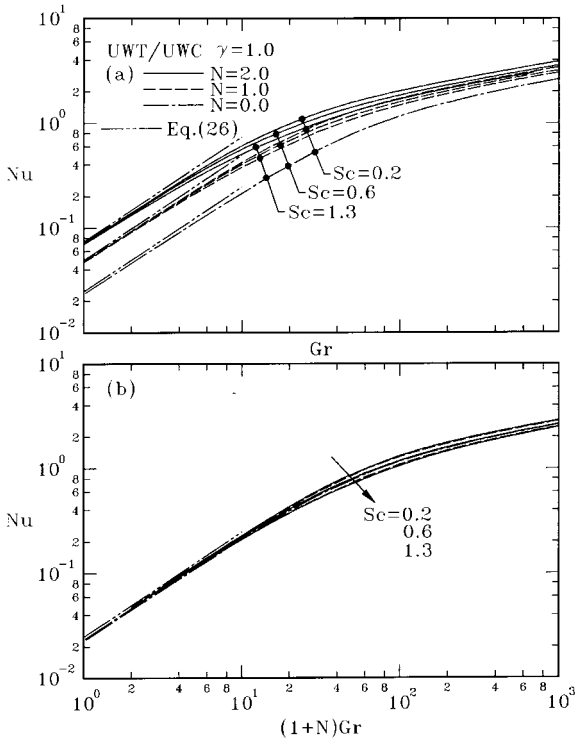

Fig. 5. Effects of buoyancy ratio N and Schmidt number Sc on the average Nusselt number for the case of UWT/UWC with $\gamma = 1$.

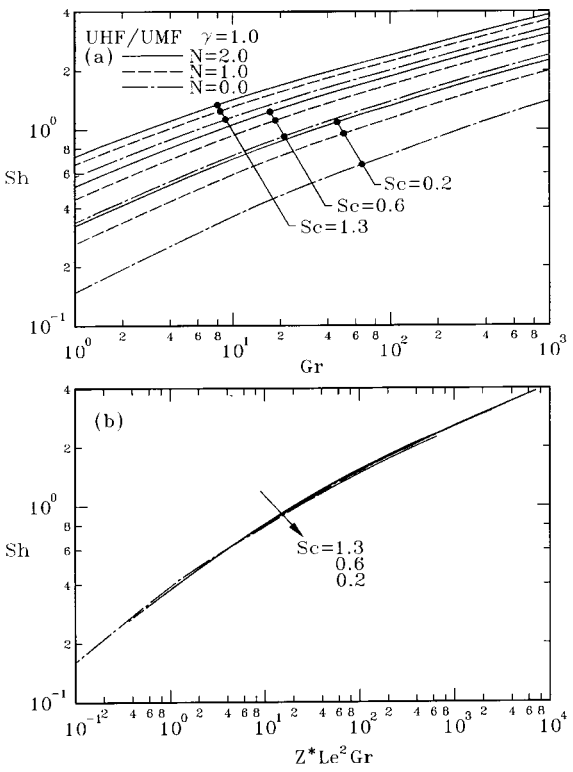

Fig. 6. Effects of buoyancy ratio N and Schmidt number Sc on the average Sherwood number for the case of UHF/UMF with $\gamma = 1$.

rate, the deviations of Nu caused by the mass diffusion effects are more significant for the case of UHF/UMF. In Fig. 4(b), in terms of $Z^*\ Gr$, the curves for various values of N and Sc collapse to a single asymptotic curve except for $N^*\ Gr > 200$. The Nu of the UHF/UMF case can be correlated by the following equation:

$$Nu = \frac{0.37874\eta^{0.62}}{(1 + 0.39558\eta^{0.756})^{1/1.8}} \quad \text{(UHF/UMF)} \tag{30}$$

where $\eta = Z^*\ Gr$ and $Z^* = 1 + N/Le$. For the UWT/UWC case in Fig. 5(b), a different perspective of the situation may be explored by plotting Nu vs $(1+N)Gr$. In this case, the results of smaller $(1+N)Gr$ collapse to single asymptotic curve, Eq. (22), and are independent of Sc and N. In addition, the curves of various Sc are nearly indistinguishable at large $(1+N)Gr$. A correlation between Nu and $(1+N)Gr$ for various combinations of Sc and N in the case of UWT/UWC can be found as

$$Nu = \frac{C_1\eta^{0.982}}{(1 + C_2\eta^{1.2996})^{1/1.8}} \quad \text{(UWT/UWC)} \tag{31}$$

where $\eta = (1+N)Gr$ and the constants C_1 and C_2 are listed in Table 1.

The effects of Sc and N on the Sh for the cases of UHF/UMF and UWT/UWC are shown in Figs. 6 and 7, respectively. For a given value N, a larger Sh are associated with the system with a larger Sc. That is, the mass transfer rate increases with increasing Sc. The reason is due to the fact that a larger Sc corresponds to a smaller binary diffusion coefficient in a given binary mixture. Hence, a thinner concentration boundary-layer thickness relative to the flow boundary-layer thickness occurs for this situation and thereby results in a larger concentration gradient at wall, which in turn, enhances the mass transfer rate. When N is decreased, the species concentration difference is small compared with the temperature difference, the Sherwood number is seen to increase rapidly. For a higher Sc, doubling N from 1 to 2 has little impact on the Sh due to the relatively low diffusivity of the mass transfer. In terms of $Z^*\ Le^2\ Gr$, the Sh for different values of N and Sc nearly collapse to a single curve (as shown in Fig. 6(b)), which can be expressed by the following correlation equation:

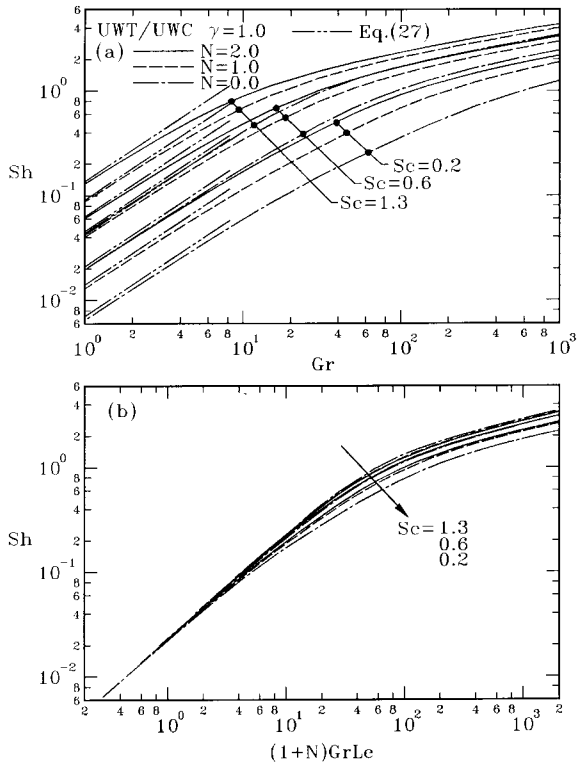

Fig. 7. Effects of buoyancy ratio N and Schmidt number Sc on the average Sherwood number for the case of UWT/UWC with $\gamma = 1$.

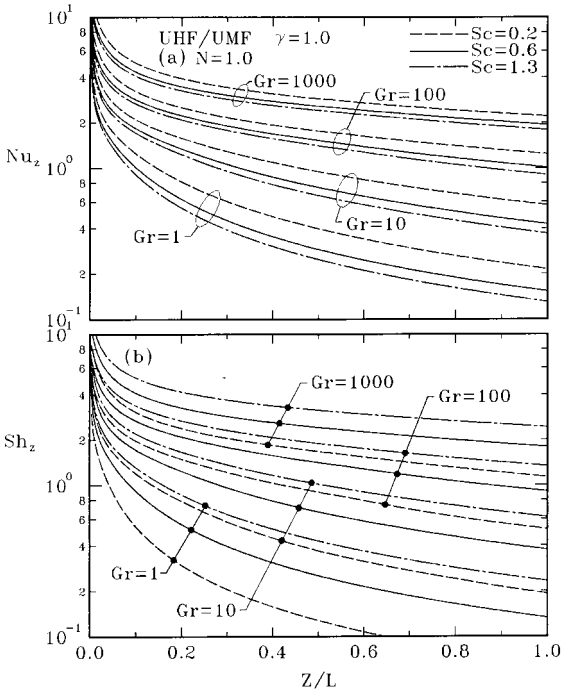

Fig. 8. The axial distributions of the local Nusselt and Sherwood numbers for the case of UHF/UMF with $\gamma=1$.

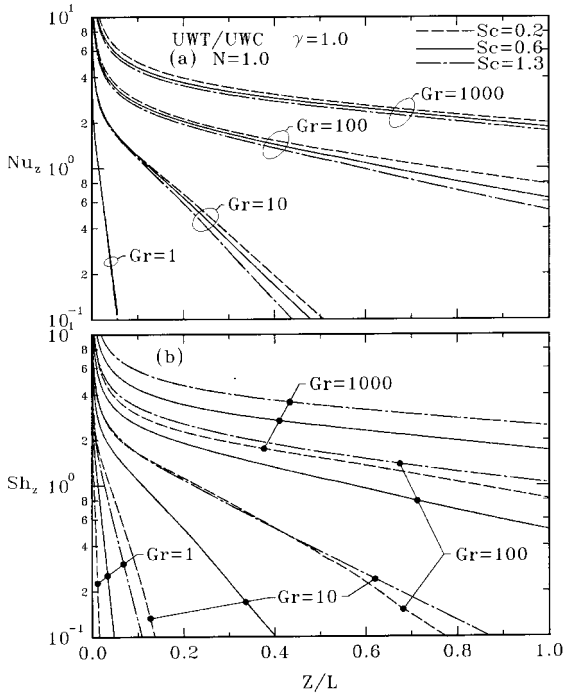

Fig. 9. The axial distributions of the local Nusselt and Sherwood numbers for the case of UWT/UWC with $\gamma=1$.

$$Sh=\frac{0.4573\eta^{0.4}}{(1+0.41345\eta^{0.378})^{1/1.8}} \quad \text{(UHF/UMF)} \tag{32}$$

where $\eta=Z^*\ Le^2\ Gr$ and $Z^*=1+N/Le$. For the UWT/UWC case, the Sh against $(1+N)Gr\ Le$ approaches a single curve at small $(1+N)Gr\ Le$. But this is not the case for large $(1+N)Gr\ Le$. The correlation equation for various combinations of N and Sc in Fig. 7(b) may be written as

$$Sh=\frac{C_1\eta^{0.995}}{(1+C_2\eta^{1.3104})^{1/1.8}} \quad \text{(UWT/UWC)} \tag{33}$$

where $\eta=(1+N)Gr\ Le$ and the constants C_1 and C_2 are listed in Table 1.

Now, attentions are focused on the axial distributions of local Nusselt and Sherwood numbers. The axial variations of Nu_z and Sh_z with Gr and Sc as parameters in the typical case (N = 1.0) for the cases of UHF/UMF and UWT/UWC are shown in Figs. 8 and 9, respectively. In Fig. 8, the Nu_z and Sh_z decrease with axial location due to the entrance effect. Smaller Nu_z and Sh_z are found for the case of lower Gr. Additionally, an increase in Sc causes a decrease in Nu_z and increase in Sh_z for a fixed Gr due to the

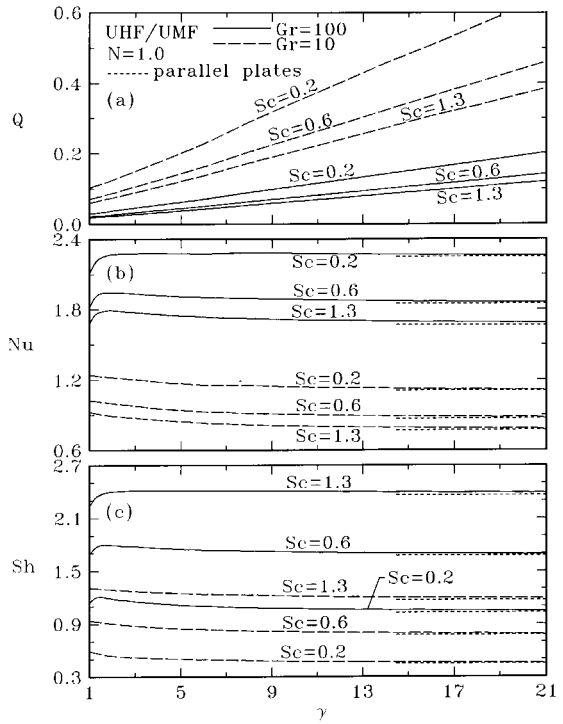

Fig. 10. Effects of aspect ratio γ on the dimensionless induced volume rate, average Nusselt and Sherwood numbers for the case of UHF/UMF.

reason stated previously. Careful inspection of Fig. 8 shows that the discrepancy of Nu_z and Sh_z between various Sc increases with decreasing Gr. For the UWT/UWC case in Fig. 9, as the Gr decreases the fluid temperature and concentration attain the uniform surface temperature and concentration on the heated wall. Hence, the Nu_z and Sh_z decrease sharply to zero, especially for the system with a smaller Gr. Relative to the UHF/UMF case, the differences of Nu_z and Sh_z between various Gr are more significant for the UWT/UWC case.

The effects of the duct aspect ratio γ on the induced volume flow rate, the average Nusselt number and the average Sherwood number are of interest. The variations of Q, Nu and Sh with aspect ratio γ as parameter for the UHF/UMF case are shown in Fig. 10. In these subplots, the results of $Gr = 10$ and 100 with various values of Sc are presented. An examination of Fig. 10(a) reveals that the Q for various combinations of Sc and Gr increases monotonically with increasing γ. The slope of each curve is nearly constant for $\gamma > 7$. In Figs. 10(b) and (c), for the results of $Gr = 100$, the curves of Nu and Sh reach maximum value at a certain value of γ, then the curves decrease with increasing γ. Finally, the Nu and Sh approach asymptotically to attain their parallel plates flow limit [15,16]. But in the case of $Gr = 10$, the results of Nu and Sh decrease with an increase in γ with maximum values at $\gamma = 1$. The effects of γ on the Q, Nu and Sh for the UWT/UWC case are shown in Fig. 11. Similar to the results of the UHF/UMF case, the variations of Q for the UWT/UWC case increase with γ. The slope of each curve is also nearly constant for $\gamma > 7$. It is also observed that the effect of Sc on the variations of Nu at different γ is nearly insignificant for $Gr = 10$. Comparing Figs. 10 and 11 reveals that the effect of γ on the Q is more significant for the UHF/UMF case than the UWT/UWC case, especially for the case of lower Gr. But the trend is reversed for the variations of Nu and Sh. Additionally, the variations of Nu and Sh for the UWT/UWC case would approach the results of parallel plates limit as $\gamma > 31$.

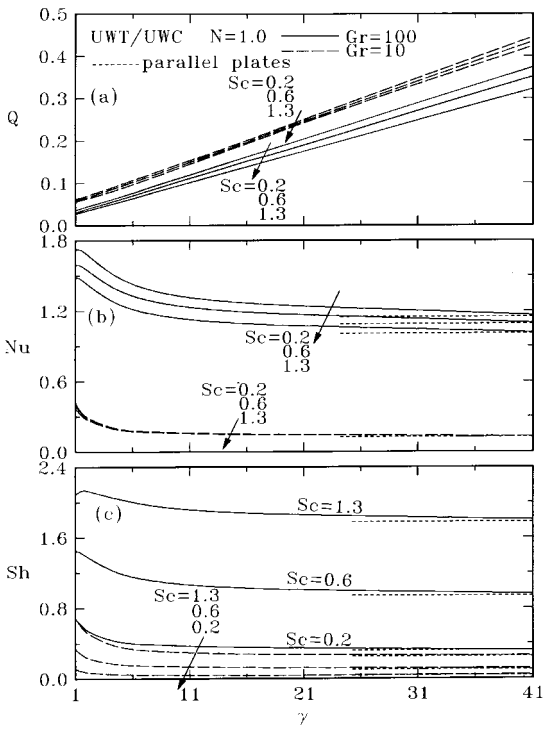

Fig. 11. Effects of aspect ratio γ on the dimensionless induced volume rate, average Nusselt and Sherwood numbers for the case of UWT/UWC.

6. Conclusions

The characteristics of natural convection heat and mass transfer in vertical rectangular ducts have been studied numerically. Analytical equations for dimensionless induced volume rate, the average Nusselt number and Sherwood number are also derived for the fully developed flow. The following conclusions can be drawn from the present analysis.

1. The Q, Nu and Sh were found to increase with buoyancy ratio N.
2. An increase in Sc causes a decrease in Q and Nu, and an increase in Sh under the same value of N.
3. The deviations of Q, Nu and Sh between various values of N and Sc are more significant for the UHF/UMF case.
4. The effects of γ on the Q are more pronounced for the UHF/UMF case than the UWT/UWC case.
5. The characteristics of natural convection in vertical rectangular ducts would approach those of two-dimensional vertical parallel plate ducts as the aspect ratio $\gamma > 31$.

References

[1] F.A. Bottemanne, Theoretical solution of simultaneous heat and mass by free convection about a vertical flat plate, Applied Scientific Journal 25 (1971) 137–149.
[2] B. Gebhart, L. Pera, The nature of vertical natural convection flows resulting from the combined buoyancy effects of thermal and mass diffusion, International Journal of Heat and Mass Transfer 14 (1971) 2025–2050.
[3] L. Pera, B. Gebhart, Natural convection flows adjacent to horizontal surfaces resulting from the combined

buoyancy effects of thermal and mass diffusion, International Journal of Heat and Mass Transfer 15 (1971) 269–278.
[4] G.D. Gallahan, W.J. Marner, Transient free convection with mass transfer on an isothermal flat plate, International Journal of Heat and Mass Transfer 19 (1976) 165–174.
[5] V.M. Soundalgeker, P. Ganesan, Finite-difference analysis of transient free convection with mass transfer on an isothermal vertical flat plate, International Journal of Engineering Science 19 (1981) 757–770.
[6] V.M. Soundalgeker, P.D. Warve, Unsteady free convection flow past an infinite vertical plate with constant suction and mass transfer, International Journal of Heat and Mass Transfer 20 (1977) 1363–1373.
[7] T.S. Chen, C.F. Yuh, Combined heat and mass transfer in natural convection on inclined surfaces, Numerical Heat Transfer 2 (1979) 233–250.
[8] T.S. Chen, C.F. Yuh, Combined heat and mass transfer in natural convection along a vertical cylinder, International Journal of Heat and Mass Transfer 23 (1980) 451–461.
[9] J. Srinivasan, D. Angirasa, Numerical study of double-diffusive free convection from a vertical plate, International Journal of Heat and Mass Transfer 31 (1988) 2033–2038.
[10] H.T. Lin, C.M. Wu, Combined heat and mass by laminar natural convection from a vertical plate with uniform heat flux and concentration, Heat and Mass Transfer 32 (1997) 293–299.
[11] H.T. Lin, C.M. Wu, Combined heat and mass by laminar natural convection from a vertical plate, Heat and Mass Transfer 30 (1995) 369–376.
[12] W.N. Gill, E.D. Casal, D.W. Zeh, Binary diffusion and heat transfer in laminar convection boundary layers on a vertical plate, International Journal of Heat and Mass Transfer 8 (1965) 1131–1151.
[13] J.C. Mollendof, B. Gebhart, Asymmetric natural convection flows resulting from the combined buoyancy effects of thermal and mass diffusion., in: Proc. 5th International Heat Transfer Conference, Tokyo, 1974 No. CT 1.3.
[14] T.S. Lee, P.G. Parikh, A. Acrivos, D. Bershadar, Natural convection in a vertical channel with opposing buoyancy forces, International Journal of Heat and Mass Transfer 25 (1982) 499–511.
[15] D.J. Nelson, B.D. Wood, Combined heat and mass transfer natural convection between vertical parallel plates, International Journal of Heat and Mass Transfer 32 (1989) 1779–1787.
[16] D.J. Nelson, B.D. Wood, Combined heat and mass transfer natural convection between vertical parallel plates with uniform flux boundary conditions, Heat and Mass Transfer 4 (1986) 1587–1592.
[17] D.J. Nelson, B.D. Wood, Fully developed combined heat and mass transfer natural convection between vertical parallel plates with asymmetric boundary conditions, International Journal of Heat and Mass Transfer 32 (1989) 1789–1792.
[18] K. Ramakrisha, S.G. Rubin, P.K. Khosla, Laminar natural convection along vertical square ducts, Numerical Heat Transfer 5 (1982) 59–79.
[19] F.C. Chou, G.J. Hwang, Vorticity–velocity methods for the Graetz problem with the effect of natural convection in a horizontal rectangular channel with uniform wall heat flux, ASME Journal of Heat Transfer 109 (1987) 704–710.
[20] P.J. Roche, in: Computational Fluid Dynamics, Reinhold, New York, 1971, pp. 61–64.
[21] W.M. Yan, Developing flow and heat transfer in radially rotating rectangular ducts with wall-transpiration effects, International Journal of Heat and Mass Transfer 37 (1994) 1465–1473.
[22] K.T. Lee, Natural convection in vertical parallel plates with an unheated entry or unheated exit, Numerical Heat Transfer 25 (1994) 477–493.
[23] A. Moutsoglou, M.R. Park, Natural convection heat transfer in a three-dimensional duct, Journal of Thermophysics and Heat Transfer 7 (1993) 369–376.